Contents lists available at SciVerse ScienceDirect

Biomaterials

journal homepage: www.elsevier.com/locate/biomaterials

Modeling vascularized bone regeneration within a porous biodegradable CaP scaffold loaded with growth factors

Xiaoqiang Sun [a,b], Yunqing Kang [c], Jiguang Bao [a], Yuanyuan Zhang [d,*], Yunzhi Yang [c,**], Xiaobo Zhou [b,***]

[a] School of Mathematical Science, Beijing Normal University, Beijing 100875, PR China
[b] Department of Radiology, Wake Forest University School of Medicine, Medical Center Boulevard, Winston-Salem, NC 27157, USA
[c] Department of Orthopedic Surgery, Stanford University, 300 Pasteur Drive, Edwards R155, Stanford, CA 94305, USA
[d] Wake Forest Institute for Regenerative Medicine, Wake Forest University School of Medicine, Medical Center Blvd., Winston-Salem, NC 27157, USA

ARTICLE INFO

ABSTRACT

Osteogenetic microenvironment is a complex constitution in which extracellular matrix (ECM) molecules, stem cells and growth factors each interact to direct the coordinate regulation of bone tissue development. Importantly, angiogenesis improvement and revascularization are critical for osteogenesis during bone tissue regeneration processes. In this study, we developed a three-dimensional (3D) multi-scale system model to study cell response to growth factors released from a 3D biodegradable porous calcium phosphate (CaP) scaffold. Our model reconstructed the 3D bone regeneration system and examined the effects of pore size and porosity on bone formation and angiogenesis. The results suggested that scaffold porosity played a more dominant role in affecting bone formation and angiogenesis compared with pore size, while the pore size could be controlled to tailor the growth factor release rate and release fraction. Furthermore, a combination of gradient VEGF with BMP2 and Wnt released from the multi-layer scaffold promoted angiogenesis and bone formation more readily than single growth factors. These results demonstrated that the developed model can be potentially applied to predict vascularized bone regeneration with specific scaffold and growth factors.

Published by Elsevier Ltd.

1. Introduction

Tissue-engineered bone regeneration [1–3] is a complex biological and medical event which includes the scaffolds themselves, cellular and signaling cues, and vascularization, as well as interactions between them [4]. Many in vitro and/or in vivo experimental studies have been conducted to determine strategies promoting osteogenesis and angiogenesis [4,5]. But due to the complexity of the process of bone regeneration within scaffolds, such coordinated processes involved in bone regeneration have often been examined piecemeal rather than systematically.

Calcium phosphate (CaP) scaffolds (e.g. beta-tricalcium phosphate [6], hydroxyapatite [7] and their composites [8]) are ideal materials for bone repair due to their biocompatibility, adjustable degradation rates, and excellent bioactivity [9,10]. When used as scaffolds for bone repair, biodegradable CaP scaffolds often contain human primary cells (e.g. mesenchymal stem cells [MSC], osteocytes, and endothelial cells) and growth factors or cytokines to repair bone tissue. Growth factors (e.g. bone morphogenetic protein 2 (BMP2), transforming growth factor β (TGFβ) and Wnt ligands) affect cellular migration and proliferation and osteogenic differentiation of MSC during bone repair. These growth factors can regulate the expression of Runt-related transcription factor 2 (Runx2) and Osterix (Osx) through intracellular proteins or transcription factors including β-Catenin, Smad1/5 and Smad2/3 [11]. Ideally, key growth factors can be programmatically encapsulated and embedded into CaP scaffolds. These cytokines are then released into the microenvironment of the bone graft after being implanted and stimulate the expression of genes responsible for the osteoblastic differentiation from MSC to pre-osteoblasts and then to active osteoblasts [11] through a variety of signaling pathways [11–14].

Besides osteoblastic differentiation promoted by growth factors released from the porous CaP scaffold, sustained bone formation needs adequate new blood vessel growth to provide nutrients to cells in the interior of the CaP scaffold. Recently, angiogenesis has

* Corresponding author. Fax: +1 336 713 7290.
** Corresponding author. Fax: +1 650 721 3470.
*** Corresponding author. Fax: +1 336 713 1789.
E-mail addresses: xiaoqiangsun88@gmail.com (X. Sun), yzhang@wakehealth.edu (Y. Zhang), ypyang@stanford.edu (Y. Yang), xizhou@wakehealth.edu (X. Zhou).

been a focus of efforts to improve clinical success of bone grafts by increasing osteoblastic cell survival. Among the many growth factors in the bone microenvironment, VEGF and FGF play a critical role in initiating and sustaining vascular growth during bone healing [15].

Addressing the remaining challenges in the field of bone regeneration requires combining multiple strategies, such as scaffold fabrication, controlled drug release, and vascularization. When combined with associated experimental studies, mathematical and computational modeling potentially provides a systematic rational approach to study bone regeneration. A number of mathematical models of bone regeneration have been developed recently [16]. Geris and co-workers [17–19] proposed a continuum-type model by employing a set of partial differential equations to describe the spatio-temporal evolution of the densities of cells and the concentrations of growth factors, but these models did not include exogenous growth factor release from the biodegradable scaffolds. J.A. Sanz-Herrera and co-workers [20–22] constructed a micro-macro numerical modeling of bone regeneration using a finite element method by integrating two levels: the tissue level or macroscopic scale, and the scaffold pore level or microscopic scale. Checa and co-workers [23–25] developed a mechano-biological model using a lattice approach to simulate cell activity and investigated the effects of cell seeding and mechanical loading on vascularization and tissue formation [23].

However, none of the above models simulated exogenous growth factor release from the scaffold and cell response to such growth factors. To overcome these limitations, we propose a computational modeling approach that integrates growth factor release from the scaffold and cell response into a vascularized bone regeneration system.

Our previous study [26] described a multi-scale systems biological model that linked the intracellular and intercellular signaling pathways with dynamic cellular properties to study the combination of effects and optimal doses of cytokines on bone remodeling based on the intracellular signaling pathway. Therein, we mainly focused on responses of cells and bone mass to cytokines (including BMP2, Wnt ligands, and TGFβ) after they were released from the scaffold, but the explicit kinetics of dynamic growth factor release was not studied. Some drug release models [27–30] provide insights into the mass transport and chemical processes involved in growth factor delivery systems, although none of them have considered responses of cell activity and angiogenesis to such drug concentration changes. The present study was designed to develop a computational systems model of bone regeneration within a 3D porous biodegradable CaP scaffold by simulating osteogenesis in response to growth factor release, based on molecular mechanisms and incorporating angiogenesis and nutrient transportation. We first reconstructed the 3D bone regeneration system, and then investigated the effects of pore size and porosity on growth factor release, angiogenesis, and bone formation. Finally, we examined whether the combination of BMP2, Wnt, and VEGF promoted angiogenesis and bone formation better than single growth factors at the same doses.

2. Materials and methods

We developed a 3D multi-scale system model for bone regeneration within porous biodegradable CaP scaffolds. A continuum reaction-diffusion sub-model for exogenous growth factor release and an agent-based sub-model for cell response were coupled in our model. We applied a set of reaction-diffusion equations to model the process of growth factor release from the porous biodegradable CaP scaffold as well as nutrient transportation by the vasculature, and employed an agent-based model [31] to simulate activities of each osteoblast and endothelial cell. Our model contained four biological/physical scales from micro level to macro level: molecular, cellular, scaffold, and bone tissue scales (Fig. 1). Each scale is described below.

2.1. Molecular scale: signaling pathway

Runx2 and Osx are two crucial transcription factors in osteoblast differentiation and bone regeneration and their expression can be regulated by released growth factors, including BMP2, TGFβ and Wnt, through activation of intracellular proteins or transcription factors such as Smad1/5 (S1), Smad2/3 (S2) and β-Catenin [11]. The molecular regulatory mechanisms involved in the intracellular signaling pathway were modeled using a system of ordinary differential equations as Equations (1.1)–(1.5), please refer to our previous study [26] for more details.

$$\frac{d[S1]}{dt} = \frac{V_1 \cdot [BMP2]}{K_1 + [BMP2]} \cdot ([TotalS1] - [S1]) - d_1 \cdot [S1] \tag{1.1}$$

$$\frac{d[S2]}{dt} = \frac{V_2 \cdot [TGF\beta]}{K_2 + [TGF\beta]} \cdot ([TotalS2] - [S2]) - d_2 \cdot [S2] \tag{1.2}$$

$$\frac{d[\beta Catenin]}{dt} = a - \left(\left(\frac{[Wnt] + b}{c \cdot [Wnt] + d} \right) \cdot \left(\frac{e}{e + [\beta Catenin]} \right) + f \right) \cdot [\beta Catenin] \tag{1.3}$$

$$\frac{d[Runx2]}{dt} = \frac{V_4 \cdot [S1]}{K_4 + [S1]} + \frac{V_5 \cdot [S2]}{K_5 + [S2]} + \frac{V_6 \cdot [\beta Catenin]}{K_6 + [\beta Catenin]} - d_4 \cdot [Runx2] \tag{1.4}$$

$$\frac{d[Osx]}{dt} = \frac{V_7 \cdot [S1]}{K_7 + [S1]} + \frac{V_8 \cdot [Runx2]}{K_8 + [Runx2]} - d_5 \cdot [Osx] \tag{1.5}$$

It was assumed that the binding and/or dissociation reactions in the intracellular signaling pathway are much faster than both cellular phenotype switches and cellular population changes [32,33], so the quasi-steady state of the intracellular signaling pathway was derived (Supplementary Text S1) in this study to link the short time scale (Minutes/Hours) of the intracellular signaling pathway to the long time scale (Days) of the cellular activity.

2.2. Cellular scale: cell activities

2.2.1. Migration

MSC and pre-osteoblasts migrate along the gradient of the normalized concentration of growth factors, including BMP2 and TGFβ, and nutrient such as oxygen. The probability (P_i^{mig}) of MSC and pre-osteoblasts migrating along the i-th direction was described in Equation (2). Active osteoblasts were assumed to migrate very little [23].

$$P_i^{mig} \propto (\nabla G + \nabla N) \cdot l_i, \quad i = 1, 2, \cdots, 6 \tag{2}$$

where G and N are the concentrations of growth factors and oxygen, respectively, and l_i is the directional vector along the i-th direction. There are 6 directions for a cell to migrate in our three-dimensional lattice.

2.2.2. Differentiation

Activated Runx2 and Osx play different roles in different stages of osteoblastic lineage. Both Runx2 and Osx can promote the differentiation of MSC into pre-osteoblasts, whereas Runx2 can inhibit the differentiation of pre-osteoblasts into active osteoblasts [11,34]. The probabilities of MSC differentiating into pre-osteoblasts ($P_{MSC \rightarrow OBp}^{diff}$) and pre-osteoblasts differentiating into active osteoblasts ($P_{OBp \rightarrow OBa}^{diff}$) were related to the expression levels of activated Runx2 and Osx. We employed Hill functions to model these situations as Equations (3) and (4).

$$P_{MSC \rightarrow OBp}^{diff} = \left(\frac{V_{D1,Runx2} \cdot [Runx2]}{K_{D1,Runx2} + [Runx2]} + \frac{V_{D1,Osx} \cdot [Osx]}{K_{D1,Osx} + [Osx]} \right) \cdot p_{MSC \rightarrow OBp}^{diff} \tag{3}$$

$$P_{OBp \rightarrow OBa}^{diff} = \left(\frac{1}{1 + [Runx2]/K_{D2,Runx2}} + \frac{V_{D2,Osx} \cdot [Osx]}{K_{D2,Osx} + [Osx]} \right) \cdot p_{OBp \rightarrow OBa}^{diff} \tag{4}$$

where $p_{MSC \rightarrow OBp}^{diff}$ and $p_{OBp \rightarrow OBa}^{diff}$ are baseline probabilities of differentiation of MSC into pre-osteoblasts and differentiation of pre-osteoblasts into active osteoblasts, respectively.

2.2.3. Proliferation

MSC, pre-osteoblasts, and active osteoblasts can proliferate into their daughter cells with different probabilities [23,35]. Several growth factors, such as IGF1, can regulate the proliferation of osteoblastic cells. In our simulation, the proliferative probabilities (p^{pro}) were set as constants (please refer to Table S2) [23] without considering the explicit effects of such growth factors.

2.2.4. Apoptosis

Hyperbaric oxygen attenuates cell's apoptosis [36] and hypoxia makes apoptosis more likely [37]. The probability of apoptosis in osteoblasts was related to the concentration of oxygen (N) as described in Equation (5). Furthermore, if oxygen concentrations are below a threshold Th$_{Oxygen}$, then osteoblasts will die. The equation is
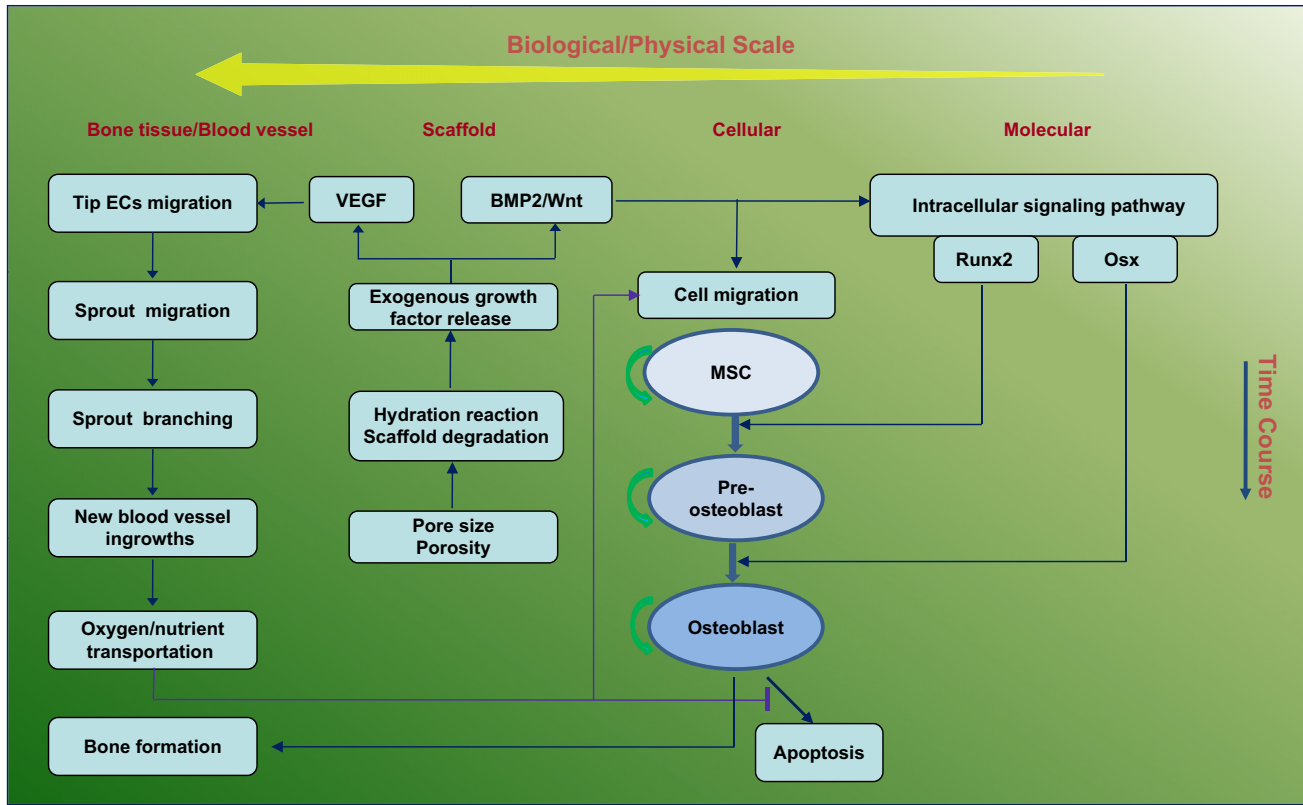
Fig. 1. Schematic representation of computational framework of 3D vascularized bone regeneration within a porous biodegradable CaP scaffold. The model encapsulates four biological/physical scales from micro level to macro level: molecular, cellular, scaffold, and bone tissue scales. At the scaffold scale, growth factors (BMP2, Wnt and VEGF) were released from the CaP scaffold via calcium phosphate degradation due to hydration reaction. At molecular scale, the released BMP2 and Wnt stimulated the intracellular signaling pathway of MSC and pre-osteoblasts to activate the transcription factors Runx2 and Osx. At the cellular scale, each osteoblastic cell underwent migration, proliferation, differentiation, and apoptosis. MSC and pre-osteoblasts migrated along the gradient of the concentration of growth factors and oxygen, and their differentiation was regulated by Runx2 and Osx. At the bone tissue scale, new capillary sprouts, migrating from host tissue, were induced and sustained by released VEGF to grow into the pores of the scaffold. The remodeled vasculature could transport oxygen to maintain osteoblast metabolism and survival within scaffold pores.

$$P^{\text{apop}} = p^{\text{apop}} + \phi(N^{\text{average}} - N) \tag{5}$$

where p^{apop} is the baseline probability of the apoptosis of MSC, pre-osteoblasts, or active osteoblasts, N^{average} is average oxygen concentration telling hyperbaric oxygen and hypoxia apart, and φ is a positive constant.

2.3. Scaffold scale: scaffold degradation and growth factor release

In bone regeneration, growth factors were encapsulated into nanospheres and loaded into porous biodegradable CaP scaffolds layer by layer. After being implanted into defected bone, calcium phosphate can degrade through hydration reaction and network breakage [38–40].

The diffusion of extracellular liquid such as water and the disintegration of the calcium phosphate network via hydrolysis are described in Equations (6) and (7) using the standard second order rate expression [28].

$$\frac{\partial C}{\partial t} = \nabla(D_C \nabla C) - k_C C M \tag{6}$$

$$\frac{\partial M}{\partial t} = -k_M C M \tag{7}$$

where C and M are water concentration and calcium phosphate molecular weight, respectively, D_C is water diffusivity, and k_C and k_M are the degradation rate constants of water and calcium phosphate, respectively. The level-set method [41] was employed to update the evolving interface of the surface-eroding CaP scaffold. More precisely, at each step in our simulation, if the calcium phosphate molecular weight decreased below a threshold level, then the corresponding bonds of the porous CaP scaffold would degrade.

Meanwhile, BMP2, Wnt ligands, and VEGF were released from the degrading CaP scaffold, and continuously diffused within the scaffold pores. The paracrine or autocrine of these cytokines, such as VEGF, were ignored as we assumed that the concentrations of these cytokines secreted by individual cells were quite low compared to that released from the CaP scaffold. The processes were modeled in the following reaction-diffusion Equation (8).

$$\frac{\partial G_i}{\partial t} = \nabla(D_{G_i} \nabla G_i) + \chi_{\text{scaffold}} r_{G_i} (G_{i,\max} - G_i) \frac{C}{C + K_C} - \chi_{\text{osteo}} u_{G_i} G_i - d_{G_i} G_i \tag{8}$$

where G_i is the concentration of each growth factor, D_{G_i} is the diffusivity of each growth factor (which varies in the regions of calcium phosphate matrix and scaffold pores), $G_{i,\max}$ is the maximum concentration of each growth factor initially loaded into the scaffold, r_{G_i} is the release constant, u_{G_i} is the depletion rate of each cytokine by osteoblasts, and d_{G_i} is the degradation rate of each cytokine. The dependence of release rate on the concentrations of water and the remaining growth factors in the CaP scaffold was modeled by using a Hill function in the second term according to the Michaelis-Menten Law [42], where K_C is the Michaelis constant.

The time-dependent characteristic function $\chi_{\text{scaffold}}(t,x)$ is equal to 1 in the calcium phosphate matrix; otherwise it is equal to 0 in the pores of the scaffolds. $\chi_{\text{osteo}}(t,x)$ is equal to 1 if a osteoblastic cell is present at x and is equal to 0 elsewhere. χ_{scaffold} and χ_{osteo} are updated at each simulation step according to the developing profiles of the porous CaP scaffold and osteoblast distribution.

Considering the tiny concentrations of growth factors within scaffold pores at the beginning of their release, the zero initial condition was applied for Equation (8). The non-dimensional initial concentration of water was set as 1 in the scaffold pores and 0 in calcium phosphate matrix, while the non-dimensional initial molecular weight of calcium phosphate was set as 1 only in the domain of CaP scaffold. Homogenous Neumann boundary conditions were imposed for all the above equations by assuming zero flux along the boundary of the considered domain. We solved these equations numerically with the finite difference method [43].

2.4. Bone tissue scale: angiogenesis, oxygen transportation, and bone formation

2.4.1. Angiogenesis

We assumed that the motion of an individual endothelial cell located at the tip of a capillary sprout governed the motion of the whole sprout, and chemotaxis in response to VEGF gradients guided the motion of the endothelial cells at the capillary sprout tip [44].

We defined the probability of migration of endothelial cells as

$$P_k \propto \alpha \frac{k_V}{k_V + V} \nabla V \cdot l_k, \quad k = 1, 2, \cdots, 6 \qquad (9)$$

where V is the concentration of VEGF, l_k is the directional vector along the k-th direction, α is the chemotactic coefficient, and k_V is a positive constant controlling the weight of VEGF concentrations in chemotactic sensitivity.

For a given tip endothelial cell at location (i,j,k), the un-normalized migration probabilities $P_1, P_2 \ldots$ and P_6 can be calculated from Equation (9). The un-normalized probability P_7 (for a tip cell to remain stationary) is the average of $P_1, P_2 \ldots$ and P_6. After normalization, the above probabilities give the likelihood of a given tip endothelial cell to move up, down, right, or left; to the front or the back; or to remain in its current position.

We then normalized the above numbers: $\bar{P}_i = P_i / \sum_{j=1}^{7} P_j$, $i = 1, 2, \ldots, 7$ and defined interval $I_1 = (0, \bar{P}_1]$, $I_i = (\sum_{j=1}^{i-1} \bar{P}_j, \sum_{j=1}^{i} \bar{P}_j)$, $i = 2, \ldots, 7$. For every sprout tip cell, we checked whether the age of vessel exceeded 18 h and whether there were enough free sites in its nearest neighborhood. If the above conditions were satisfied, two random numbers r_1 and r_2 between 0 and 1 were generated. If $r_1 \in I_2$ and $r_2 \in I_3$, then we moved two endothelial cells, one down and another to the front of the sprout tip endothelial cell. If the above branching conditions were not satisfied, we generated another random number r between 0 and 1. If $r \in I_5$, we moved the tip endothelial cell to the right of the sprout tip endothelial cell. If two sprouts encountered each other, a new sprout continued to grow.

2.4.2. Nutrient transportation

Oxygen can be transported by the neo-vasculature to osteoblasts within scaffold pores, which is described in Equation (10).

$$\frac{\partial N}{\partial t} = D_N \Delta N + \chi_{ves}(t,x) q_N \left(N^{blood} - N \right) - \chi_{osteo}(t,x) u_N N \qquad (10)$$

where N is oxygen concentration, D_N is oxygen diffusivity, q_N is the vessel permeability for oxygen, N^{blood} is blood oxygen concentration, and U_N is a cell's uptake rate of oxygen. χ_{ves} and χ_{osteo} are the characteristic functions as described above. The initial concentration of oxygen was assumed as the average concentration of oxygen within the scaffold. Homogenous Neumann boundary condition was also set for the above equation by assuming zero flux along the boundary of the considered domain.

2.4.3. Bone mass growth

The growth rate of bone mass is assumed to be proportional to the number of active osteoblasts, so we used the cumulative number of active osteoblasts as the relative measure of the bone mass at the designated time.

2.5. Model implementation

The time-course of bone formation and vascularization within the scaffold was modeled as an iterative process. Here, we summarize our computing algorithm at each step across multi-scales as follows. At the scaffold scale, we solved Equations (6)–(8) to obtain the spatial distributions of diffusing water concentration, calcium phosphate molecular weight and concentrations of released growth factors. At molecular scale, we used the calculated local BMP2 and Wnt concentrations at each lattice point as the input of the Equation (1) for intracellular signaling pathway for each osteoblast. At the cellular scale, the migration of MSC and pre-osteoblasts was simulated according to Equation (2); meanwhile, the differentiation of MSC and pre-osteoblasts was regulated by Equations (3) and (4), and the proliferation and apoptosis of osteoblastic cells were simulated accordingly. At the bone tissue scale, the spatial concentration distributions of VEGF (Equation (8)) will guide the tip endothelial cells' migration and sprout branching (Equation (9)). In turn, the remodeled vasculature at tissue scale influences the spatial concentration distributions of oxygen (Equation (10)) within CaP scaffold pores.

We performed our simulation on a three-dimensional cubic lattice. The lattice size was set to $50 \times 50 \times 50$, representing a 1.5 mm $\times$ 1.5 mm $\times$ 1.5 mm portion of the porous biodegradable CaP scaffold. Each lattice point represented a possible space for cells to occupy. The lattice spacing was 30 μm, the approximate diameter of an osteoblast. The endothelial cells are usually smaller, thus we assumed that the neo-vasculature were not particularly closely packed. Each time step of iterative-process simulated the real time length of 1 day. Initially the scaffold was assumed to be loaded with growth factors (e.g. BMP2, Wnt ligands, and VEGF), and the pores of the scaffold were assumed to be filled with granulation tissue and MSCs were seeded inside the construct. The pore sizes (pore diameters) of different scaffolds ranged from 180 μm to 720 μm by intervals of 60 μm for different simulations. The pores in each type of scaffolds were arranged uniformly with equal distance between inter-pores. In addition, two parent blood vessels were initialized on the up and down layers of the lattice.

The program was performed in MATLAB R2007b (MathWorks) on a DELL computer (Intel (R) Core (TM) i5-3470 CPU @ 3.20 GHz/16.0 GB RAM). The average running time of a typical simulation was 23 min. Tables S1 and S2 list the parameters used in the model. Most were found in the literature [31,45–47], and some parameters involved in the growth factor release module, including degradation rates

of water (k_C) and molecular weight of scaffold material CaP (k_C), and growth factor release constant (r_{G_i}) (please refer to Table S2), were determined by fitting them to our experimental data described below.

2.6. Experimental study of BMP2 release

In the experiment, purified BMP-2 was dissolved with sterile PBS containing 1% bovine serum albumin (BSA) to make a BMP-2 solution, in which the 1% BSA was used to stabilize BMP-2 and inhibit nonspecific adsorption of BMP-2. Each scaffold was immersed in 150 μl BMP-2 solution containing 50 μg of BMP-2 overnight at 4 °C. BMP-2 loaded CaP scaffolds were placed into silanized 24-well culture plates. 2 ml of tissue culture medium was added into each well and incubated in a humidified 95% air, 5% CO_2 atmosphere at 37 °C. 1.2 ml of the tissue culture medium was collected for the BMP elution assay, and then 1.2 ml fresh culture medium was added to the plates to maintain the constant volume (2 ml) of medium at 1, 3, 5, 7 and 14 days. The release was assayed at designated time points. Concentrations of BMP-2 in the removed solution were analyzed using a human BMP-2 ELISA development kit (PeproTEch Inc., Rock Hill, NJ). The degree of BMP-2 release was considered as the BMP-2 concentration of removed solution. Measurements were performed in triplicate for each time point.

3. Results

First, we reconstructed the 3D bone regeneration system, and then investigated the effects of pore size and porosity of the scaffold on growth factor release, angiogenesis, and bone formation. Finally, we examined the effects of combining growth factors.

3.1. Baseline simulation of 3D vascularized bone regeneration

First, we reconstructed the system of vascularized bone regeneration within the 3D porous CaP scaffold, which involved the coupled processes of evolution of scaffold degradation, exogenous growth factor release, angiogenesis, MSC differentiation, and cell growth within scaffold pores over time. Fig. 2 shows a typical simulation of our 3D modeling. On day 7, the blood vessels were rare and scattered on the outside surface of the porous CaP scaffold; on days 14 and 21, the newly formed blood vessels grew into the pores located at the periphery of the scaffold. Simultaneously, some blood vessels branched into clusters of tree-branching capillaries. On day 28, a branched vasculature was observed within the peripheral pores of the scaffold. Few blood vessels were predicted to grow into the pores at the center of the scaffold.

The uniformly distributed pores on the scaffolds gradually enlarged due to biodegradation of the scaffold. At early stages, MSC originally recruited from the host filled in the 3D scaffold pores. MSC gradually differentiated into pre-osteoblasts and active osteoblasts, and then active osteoblasts outnumbered MSC and pre-osteoblasts within the scaffold pores.

Fig. 3 shows a 2D cross-sectional view of the spatio-temporal evolution of BMP2, VEGF, and oxygen concentrations; CaP molecular weight; and scaffold/cell profiles near the top layer of the scaffold on days 1, 7, 14, 21, and 28. BMP2 and VEGF were released from the calcium phosphate matrix and continuously diffused in the scaffold pores, and concentrations of these growth factors in the pores of the scaffold increased over time. In our simulation, the maximum concentration of VEGF initially loaded into the biodegradable CaP scaffold was higher in the center of the scaffold and lower in the periphery, so a gradient of VEGF concentration within the pores was produced as it was released from the scaffold. Our simulation also demonstrated that the scaffold with gradient VEGF loading can promote angiogenesis much more than the scaffold with uniform VEGF loading. The oxygen concentration changed along with cells' uptake and the transportation of oxygen in the neo-vasculature. The molecular weight of calcium phosphate decreased from day 1 to day 28 due to hydrolysis.

Fig. 4 shows how numbers of various cells changed over time in the model. At first, MSC, pre-osteoblasts, and active osteoblasts all
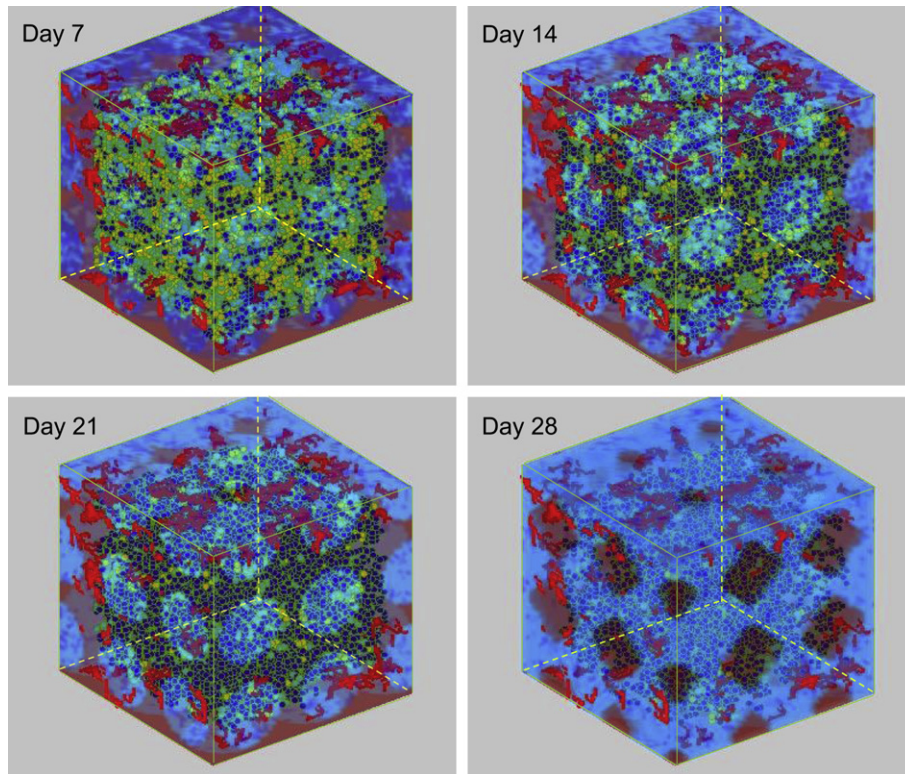
Fig. 2. A typical simulation from a 3D model showing the evolution of scaffold resorption, angiogenesis, MSC differentiation, and cell growth within scaffold pores over time. Different colors denote various cell types: yellow (MSC), green (pre-osteoblasts), blue (active osteoblasts), and red (blood vessels). The uniformly distributed pores on the scaffolds gradually degraded due to resorption of the scaffold. Newly formed blood vessels grew into the pores at the periphery of the scaffold. (For interpretation of the references to color in this figure legend, the reader is referred to the web version of this article.)

increased; once they each achieved a peak level, they decreased due to differentiation and/or apoptosis. Numbers of different cell types peaked at different times, consistent with the development of the osteoblast phenotype through osteoblast lineage [48,49]. The numbers of MSC peaked at around day 3, pre-osteoblasts achieved their peak on day 7, and active osteoblasts peaked on day 14. The number of endothelial cells increased throughout the simulation.

A video showing the dynamic evolution of 3D vascularized bone regeneration within a porous CaP scaffold is included in the Supplementary Materials (Movie S1).

Supplementary data related to this article can be found online at http://dx.doi.org/10.1016/j.biomaterials.2013.03.015.

3.2. Tailoring growth factor release profile by controlling scaffold pore size

Fig. 5 shows cumulative released BMP2 from scaffolds with a small pore size (480 μm) or a large pore size (720 μm), respectively. The 480 μm pore scaffold has a faster release rate and higher release fraction of BMP2 compared to the 720 μm pore scaffold. This simulation was validated by our experimental data. The mean squared errors of our prediction were 0.0216 for the smaller pore size scaffold and 0.0295 for larger pore size scaffold, respectively. The good agreement between the simulation prediction and experimental data provided an important validation of our model.

Fig. 6 demonstrates the release profiles of BMP2 from scaffolds with pore sizes ranging from 180 μm to 720 μm. Initially, all scaffolds were loaded with the same amount of BMP2. The scaffolds with smaller pore sizes showed a faster release rate and greater amount of BMP2 released, compared to the larger pore sizes. These results suggest that growth factor release rate and release fraction

can be tailored, by controlling the pore size of scaffold, to achieve the specific goals of growth factor release or drug delivery in bone tissue engineering.

3.3. Effects of porosity on angiogenesis and bone formation

Scaffold porosity in this study was calculated as the ratio of void pore volume versus total scaffold volume, and the pore size was defined as the diameter of the scaffold pores. As two critical design parameters that can be controlled in the scaffold design, the pore size and porosity were programmed as two independent factors to investigate their effects on bone regeneration. Our simulations have been conducted with different pore sizes and varied values of porosities (see Fig. 7a). Fig. 7b shows the number of endothelial cells with different pore sizes after 4 weeks and 8 weeks. There were more endothelial cells when the pore size was 420 μm or 540 μm. Correspondingly, the numbers of active osteoblasts and bone mass were greatest at week 8, when the pore size was 540 μm (Fig. 7c, d). The optimal pore size for both angiogenesis and bone formation, and greatest porosity, was 540 μm.

We also examined the correlations between the scaffold porosity and the number of active osteoblasts, endothelial cells, and bone mass. These all showed trends similar to those of scaffold porosity, and much less correlation with scaffold pore sizes (Fig. 8a). Overall, the numbers of endothelial cells and active osteoblasts, as well as bone mass, increased with scaffold porosity, showing a stronger dependence of angiogenesis and bone mass formation on scaffold porosity than on pore size (Fig. 8b).

The relationship between higher porosity and enhanced bone formation was consistent with previous reports [50–53] and with
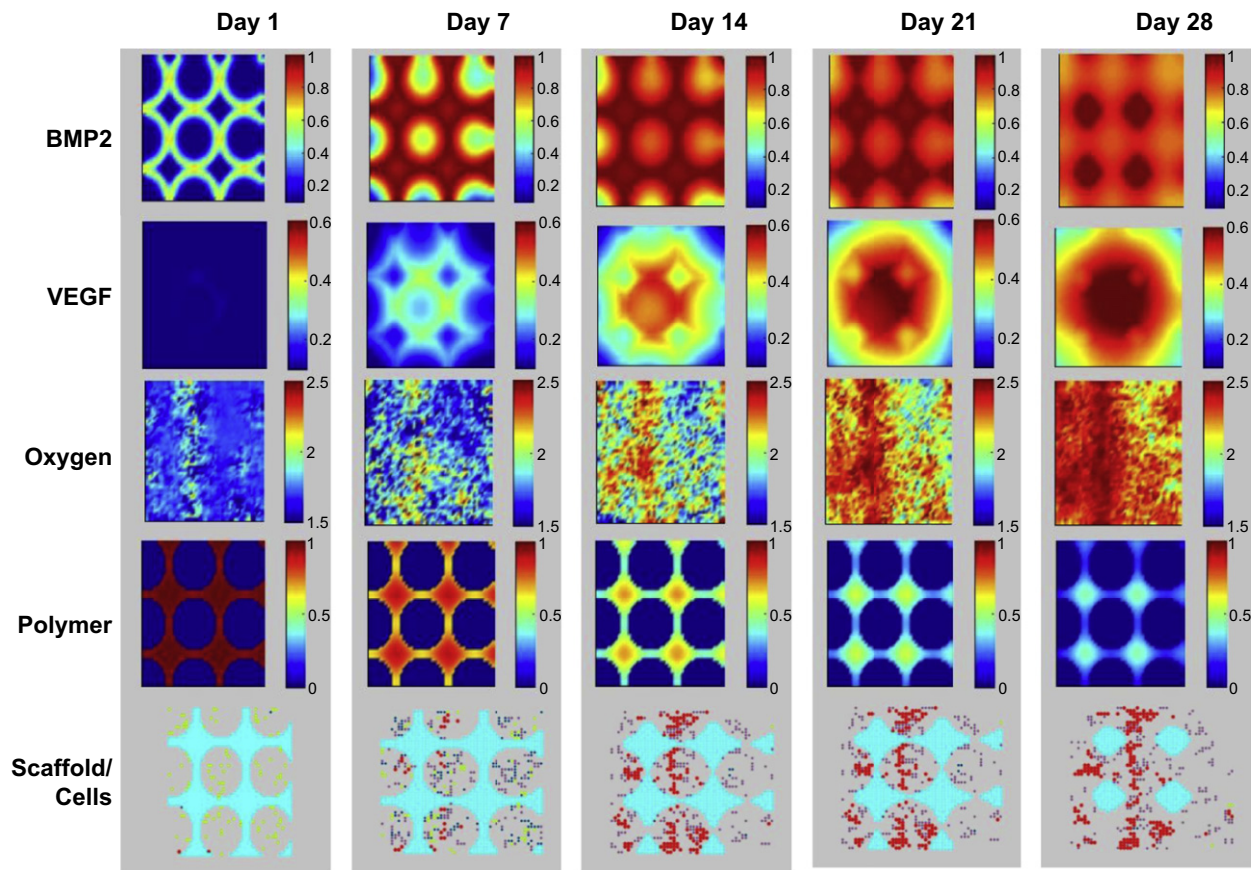
Fig. 3. 2D cross-sectional view of the spatio-temporal evolution of BMP2 concentration, VEGF concentration, oxygen concentration, calcium phosphate molecular weight, and scaffold/cell profiles over time. BMP2 and VEGF were released from the calcium phosphate matrix, and continuously diffused into the scaffold pores. Oxygen concentrations changed because of uptake by osteoblasts and transportation by the neovasculature. Calcium phosphate molecular weight decreased because of hydrolysis. Bottom row: degradation of porous CaP scaffold (cyan) and the differentiation of MSC (yellow) into active osteoblasts (blue), as well as angiogenesis (red). (For interpretation of the references to color in this figure legend, the reader is referred to the web version of this article.)
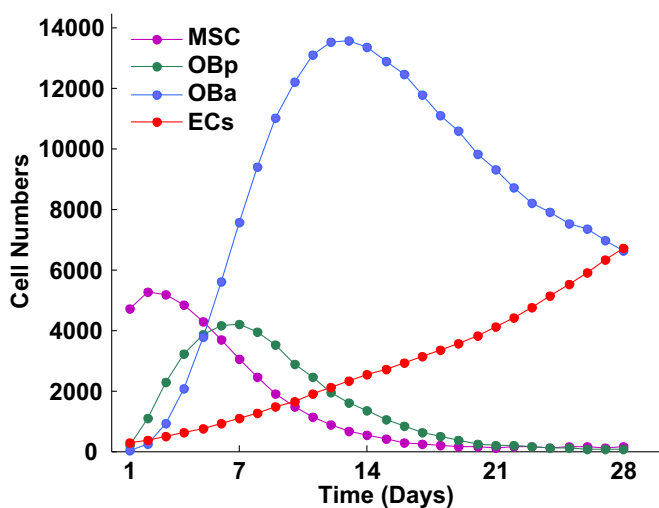

Fig. 4. Predicted changes in numbers of cell types over time. Peaks of different cell types occurred at different times, reflecting osteoblast phenotype development through the osteoblast lineage. ECs, endothelial cells; MSC, mesenchymal stem cells; OBa, active osteoblasts; and OBp, pre-osteoblasts.

experimental studies [53–55] that reported no difference in osteogenesis with different pore sizes.

3.4. Effects of combining growth factors

Finally we studied the effects of different growth factors, in single or combined form, released from the scaffold on angiogenesis and bone formation. The total doses of growth factors initially loaded into multi-layer scaffolds were the same. We examined 4 cases: In case a, 10 doses of Wnt were used; in case b, 10 doses of BMP2 were used; in case c, a combination of 4 doses of Wnt, 2 doses of BMP2 and 4 doses of VEGF was used; and in case d, a combination of 2 doses of Wnt, 4 doses of BMP2 and 4 doses of VEGF was used.

Among all four cases, using only Wnt promoted the lowest increase in active osteoblasts (Fig. 9a). When only BMP2 was used, although osteoblasts increased more quickly initially, they dropped markedly after 2 weeks, resulting in a low level of active osteoblasts after 8 weeks. The combination of Wnt, BMP2, and VEGF promoted the most efficient growth of active osteoblasts. Angiogenesis was promoted significantly when exogenous VEGF was introduced (Fig. 9b). After 8 weeks, bone formation was greatest when all 3 growth factors were combined (Fig. 9c). In addition, bone formation was faster with a higher BMP2 dose. Therefore, these results suggest that a high ratio of BMP2 when growth factors are combined may accelerate the progress and the efficiency of bone formation.
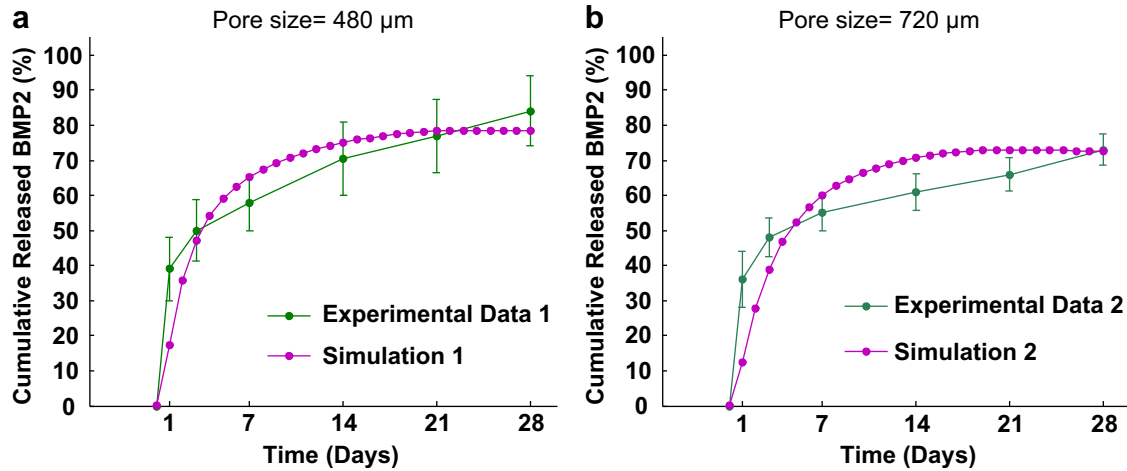
Fig. 5. Predictions of cumulative released BMP2 from scaffolds with (a) small pore size (480 μm) and (b) big pore size (720 μm), compared with our experimental data.

4. Discussion

Vascularization, important for nutrient transportation and bone implant survival, remains a major challenge in bone tissue engineering. In our simulation, we found that vascularization could be promoted by initially loading more VEGF into the center of the scaffold than in the periphery. Our simulation also demonstrated that neo-vascularization occurred at the periphery of the scaffold. One of the reasons for this was that the scaffold walls obstructed the ingrowth of new capillaries. Therefore wider spaces between the pores of the scaffold, i.e. higher interconnectivity of the pores, may improve angiogenesis in tissue engineered bone regeneration, which could be useful in guiding scaffold design.

Our model successfully captured key kinetic features of growth factor release from the CaP scaffold. We validated the simulation results with experimental data (Fig. 5). Our simulation demonstrated that scaffolds with smaller pore sizes resulted in a faster release rate and higher release of BMP2 compared to scaffolds with bigger pore sizes. This suggests the possibility of tailoring growth factor release rate and release fraction by controlling the pore size of scaffold, to reach the desired goals of drug release or drug delivery in bone tissue engineering.

We interpret the mechanism involved in this phenomenon as follows: diffusional mass transfer is one of the most important processes in drug release and delivery; therefore, diffusion of drug molecules greatly affects drug release rate. Larger pores in a scaffold means there is a larger region in which growth factor molecules can diffuse. Thus, more molecules must be released from the scaffold to fill these larger pore spaces to reach the same concentration level as the smaller pores. As a result, the average concentration of released growth factors within the bigger pores is lower than that within the smaller pores.

This work was designed to model exogenesis growth factor release and its effects on cell behavior within porous scaffold and to reveal optimal strategies for vascularized bone regeneration. Therefore we did not explicitly simulate those factors that were also important in bone regeneration. For instance, it has been shown that mechanical stimuli affects cell proliferation and differentiation as well as angiogenesis involved in bone regeneration [56], which are also important but beyond the scope of this work. Mechanical stimuli will be integrated into our multi-scale model by employing finite element method [23,24] in a follow-up study.

The assumption that the pores of the scaffold were uniformly distributed in our model will be substituted by a real scaffold structure where the pores are distributed heterogeneously, which can be achieved by using micro-CT in our future work. Some more experiments will be conducted to estimate the parameters in our model and to validate the predicted results. Some rates or probabilities regulating cell activities including differentiation, proliferation and apoptosis can be estimated from ALP and dsDNA level data. Diffusivities of growth factors and liquids (such as water) in the microenvironment of scaffold pores can be assayed using dye-labeled perfusion MRI. And intravital microscopy will be used for validating spatial distribution of cells and the growth and topology of vasculature.

Our previous study [26] examined the underlying molecular and cellular mechanisms for the cell response to released cytokines, and predicted that the combination of Wnt and BMP2 can achieve best control of bone remodeling and best bone mass regeneration among the combinations of growth factors. We also explored the optimal dose ratios of given cytokine combinations released from the scaffold to most efficiently control the long-term bone remodeling. In the present study, we show that the combination of VEGF, BMP2, and Wnt could promote osteogenesis more than BMP2 or Wnt alone, consistent with results from previous experiments [57–59].
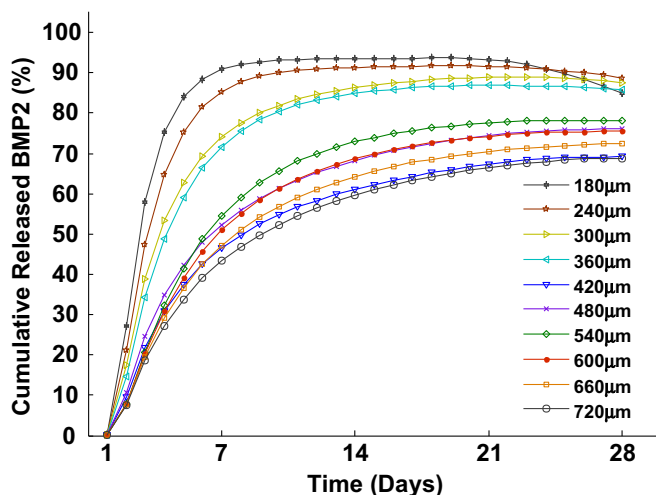

Fig. 6. Predictions of cumulative released BMP2 from scaffolds (measured by the concentration of released BMP2 in the pore space) as a function of different pore sizes.
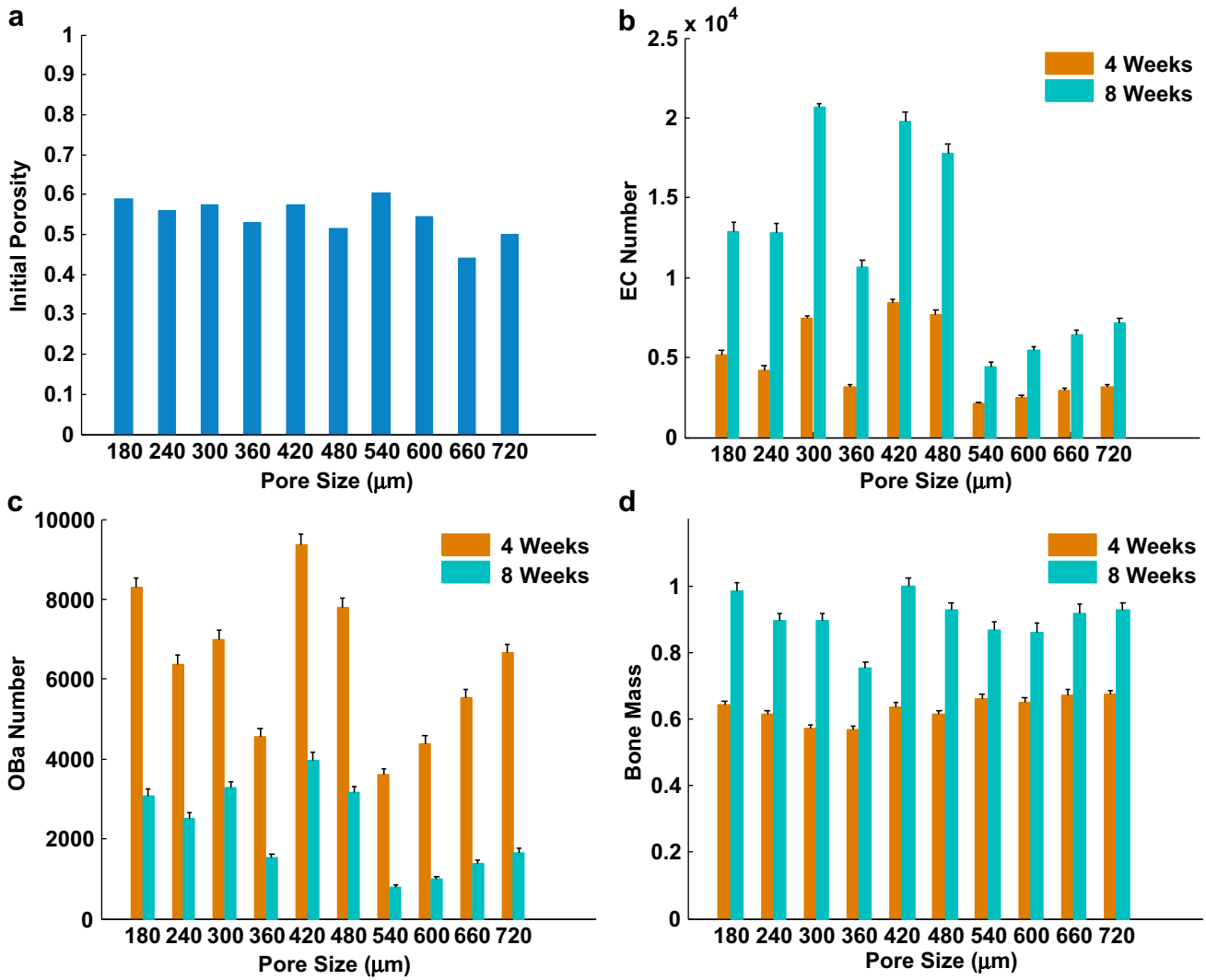
Fig. 7. Predicted effects of scaffold porosity and pore size on angiogenesis and bone formation. (a) Initial porosities of scaffolds with different pore sizes. (b) Normalized numbers of endothelial cells (c) active osteoblasts; and (d) bone mass as a function of different pore sizes after 4 and 8 weeks, respectively.
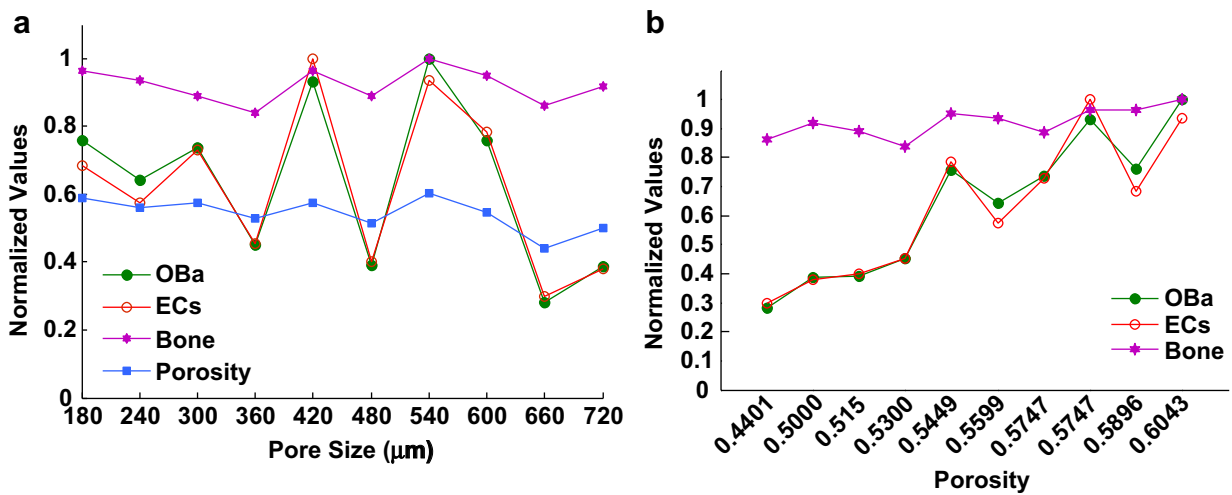

Fig. 8. The correlations between the scaffold porosity or pore size and the number of active osteoblasts, endothelial cells, and bone mass. (a) After 8 weeks, predicted numbers of active osteoblasts and endothelial cells, and bone mass formation showed a greater correlation to scaffold porosity than to scaffold pore sizes. (b) Numbers of active osteoblasts (OBa) and endothelial cells (ECs), as well as bone mass formation, were strongly related to porosity. "Normalized values" indicates that these values were normalized to their original maximum values.
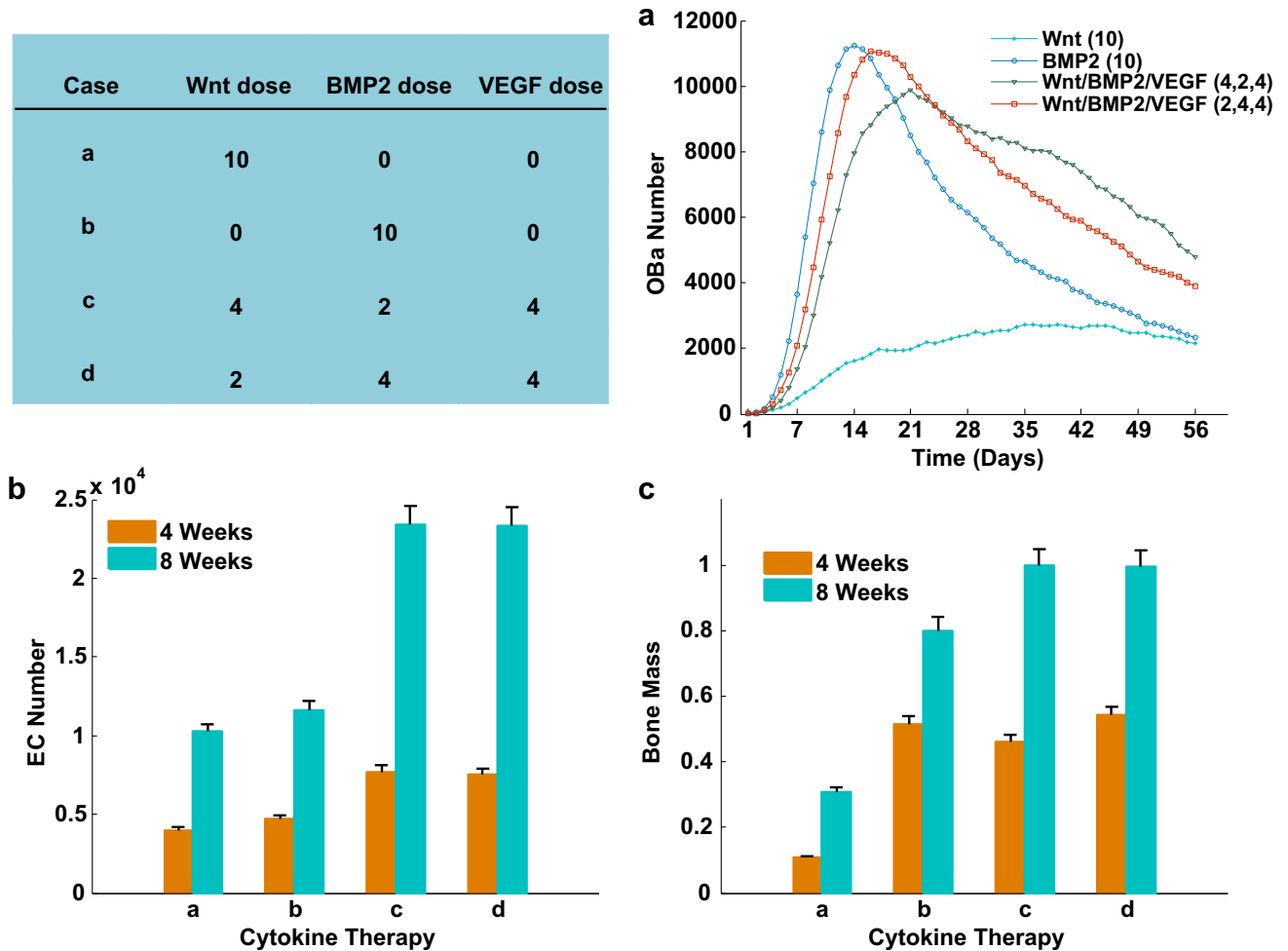
Fig. 9. Growth factor combination prediction. In therapy case a, 10 dose of Wnt was used; in therapy case b, 10 dose of BMP2 was used; in therapy case c, a combination of 4 dose of Wnt, 2 dose of BMP2 and 4 dose of VEGF were used; in therapy case d, a combination of 2 dose of Wnt, 4 dose of BMP2 and 4 dose of VEGF were used. (a) The evolution of the numbers of active osteoblasts from day 1 to day 56 under different therapies. (b) The normalized number of endothelial cells under different therapies evaluated in 4th and 8th week. (c) The normalized bone mass under different therapies evaluated in 4th and 8th week. The most efficient growth of active osteoblasts was promoted by the combination of Wnt, BMP2, and VEGF (case c and d). The number of endothelial cells increased dramatically in therapies with VEGF (case c and d) compared with therapies without VEGF (case a and b). More bone formation was observed after 8 weeks when different growth factors were combined together (case c and d) than the therapies of single growth factor (case a and b).

An ongoing experiment from our lab indicates that in mouse bone marrow stromal cells, adding BMP2 on day 1 followed by IGF1 on day 4 resulted in higher alkaline bone phosphatase concentrations and mineralization levels than other tested candidates of temporal combinations of BMP2 and IGF1. Additionally, published work [60] indicated that sequential delivery of BMP-2 and IGF-1 using a chitosan gel with gelatin microspheres could enhance early osteoblastic differentiation. These results suggest that sequential delivery of multiple cytokines using a multi-layer biodegradable scaffold can potentially improve vascularized bone regeneration. In our ongoing work, we will test other possible cytokine combinations and optimize drug doses, delivery sequence, and timing.

5. Conclusions

This study developed a 3D multi-scale model of a bone regeneration system that incorporates several coupled processes, including evolution of scaffold degradation, exogenous growth factor release, osteogenic differentiation and proliferation, angiogenesis, and nutrient transportation over time. Scaffold porosity played a more dominant role in promoting bone formation and angiogenesis compared to pore size, while the pore size could be controlled to tailor the release rate and release fraction of the exogenous growth factors. These predictions from our model were confirmed with our experimental data. Furthermore, with the same total doses, the combination of gradient VEGF plus BMP2 and Wnt released from the multi-layer scaffold promoted angiogenesis and bone formation to a much greater degree than BMP2 or Wnt alone. These results suggest that designing pore size and porosity of the scaffold, as well as combining growth factors, are critical for enhancing vascularized bone regeneration.

Abbreviations

CaP   calcium phosphate
BMP2   bone morphogenetic protein 2
VEGF   vascular endothelial growth factor
IGF1   insulin-like growth factor 1
Osx   Osterix
Runx2   Runt-related transcription factor 2
MSC   mesenchymal stem cell
OBp   pre-osteoblasts
OBa   active osteoblasts
EC   endothelial cell
3D   three-dimensional
2D   two-dimensional

Appendix A. Supplementary data

Supplementary data related to this article can be found at http://dx.doi.org/10.1016/j.biomaterials.2013.03.015.

References

[1] Petite H, Viateau V, Bensaid W, Meunier A, De Pollak C, Bourguignon M, et al. Tissue-engineered bone regeneration. Nat Biotechnol 2000;18:959–63.
[2] Dragoo JL, Lieberman JR, Lee RS, Deugarte DA, Lee Y, Zuk PA, et al. Tissue-engineered bone from BMP-2–transduced stem cells derived from human fat. Plast Reconstr Surg 2005;115:1665–73.
[3] Trautvetter W, Kaps C, Schmelzeisen R, Sauerbier S, Sittinger M. Tissue-engineered polymer-based periosteal bone grafts for maxillary sinus augmentation: five-year clinical results. J Oral Maxillofac Surg 2011;69:2753–62.
[4] Nguyen LH, Annabi N, Nikkhah M, Bae H, Binan L, Park S, et al. Vascularized bone tissue engineering: approaches for potential improvement. Tissue Eng Part B Rev 2009;15:363–82.
[5] Lovett M, Lee K, Edwards A, Kaplan DL. Vascularization strategies for tissue engineering. Tissue Eng Part B Rev 2009;15:353–70.
[6] Kim CS, Kim JI, Kim J, Choi SH, Chai JK, Kim CK, et al. Ectopic bone formation associated with recombinant human bone morphogenetic proteins-2 using absorbable collagen sponge and beta tricalcium phosphate as carriers. Biomaterials 2005;26:2501–7.
[7] Oh SH, Finones RR, Daraio C, Chen LH, Jin S. Growth of nano-scale hydroxyapatite using chemically treated titanium oxide nanotubes. Biomaterials 2005;26:4938–43.
[8] Imranul Alam M, Asahina I, Ohmamiuda K, Takahashi K, Yokota S, Enomoto S. Evaluation of ceramics composed of different hydroxyapatite to tricalcium phosphate ratios as carriers for rhBMP-2. Biomaterials 2001;22:1643–51.
[9] Yang Y, Kim KH, Ong JL. A review on calcium phosphate coatings produced using a sputtering process–an alternative to plasma spraying. Biomaterials 2005;26:327–37.
[10] El-Ghannam A. Bone reconstruction: from bioceramics to tissue engineering. Expert Rev Med Devices 2005;2:87–101.
[11] Gordeladze JO, Reseland JE, Duroux-Richard I, Apparailly F, Jorgensen C. From stem cells to bone: phenotype acquisition, stabilization, and tissue engineering in animal models. ILAR J 2009;51:42–61.
[12] Miyoshi K, Nagata H, Horiguchi T, Abe K, Arie Wahyudi I, Baba Y, et al. BMP2-induced gene profiling in dental epithelial cell line. J Med Invest 2008;55:216–26.
[13] Ryoo HM, Lee MH, Kim YJ. Critical molecular switches involved in BMP-2-induced osteogenic differentiation of mesenchymal cells. Gene 2006;366:51–7.
[14] Afzal F, Pratap J, Ito K, Ito Y, Stein JL, Van Wijnen AJ, et al. Smad function and intranuclear targeting share a Runx2 motif required for osteogenic lineage induction and BMP2 responsive transcription. J Cell Physiol 2004;204:63–72.
[15] Devescovi V, Leonardi E, Ciapetti G, Cenni E. Growth factors in bone repair. Chir Organi Mov 2008;92:161–8.
[16] Sun W, Lal P. Recent development on computer aided tissue engineering–a review. Comput Methods Programs Biomed 2002;67:85–103.
[17] Geris L, Vander Sloten J, Van Oosterwyck H. In silico biology of bone modelling and remodelling: regeneration. Philos Transact A Math Phys Eng Sci 2009;367:2031–53.
[18] Geris L, Sloten JV, Oosterwyck HV. Connecting biology and mechanics in fracture healing: an integrated mathematical modeling framework for the study of nonunions. Biomech Model Mechanobiol 2010;9:713–24.
[19] Geris L, Reed AAC, Vander Sloten J, Simpson AHRW, Van Oosterwyck H. Occurrence and treatment of bone atrophic non-unions investigated by an integrative approach. PLoS Comput Biol 2010;6:e1000915.
[20] Sanz-Herrera JA, Garcia-Aznar J, Doblare M. Simulation of bone remodelling and bone ingrowth within scaffolds. Key Eng Mater 2008;377:225–73.
[21] Sanz-Herrera J, Garcia-Aznar J, Doblare M. Micro–macro numerical modelling of bone regeneration in tissue engineering. Comput Methods Appl Mech Eng 2008;197:3092–107.
[22] Sanz-Herrera J, Garcia-Aznar J, Doblare M. A mathematical approach to bone tissue engineering. Philos Transact A Math Phys Eng Sci 2009;367:2055–78.
[23] Sandino C, Checa S, Prendergast PJ, Lacroix D. Simulation of angiogenesis and cell differentiation in a CaP scaffold subjected to compressive strains using a lattice modeling approach. Biomaterials 2009;31:2446–52.
[24] Checa S, Prendergast PJ. Effect of cell seeding and mechanical loading on vascularization and tissue formation inside a scaffold: a mechano-biological model using a lattice approach to simulate cell activity. J Biomech 2010;43:961–8.
[25] Checa S, Prendergast PJ. A mechanobiological model for tissue differentiation that includes angiogenesis: a lattice-based modeling approach. Ann Biomed Eng 2009;37:129–45.
[26] Sun X, Su J, Bao J, Peng T, Zhang L, Zhang Y, et al. Cytokine combination therapy prediction for bone remodeling in tissue engineering based on the intracellular signaling pathway. Biomaterials 2012;33:8265–76.
[27] Arifin DY, Lee LY, Wang CH. Mathematical modeling and simulation of drug release from microspheres: implications to drug delivery systems. Adv Drug Deliv Rev 2006;58:1274–325.
[28] Rothstein SN, Federspiel WJ, Little SR. A unified mathematical model for the prediction of controlled release from surface and bulk eroding polymer matrices. Biomaterials 2009;30:1657–64.
[29] Siepmann J, Gopferich A. Mathematical modeling of bioerodible, polymeric drug delivery systems. Adv Drug Deliv Rev 2001;48:229–47.
[30] Tzafriri A. Mathematical modeling of diffusion-mediated release from bulk degrading matrices. J Control Release 2000;63:69–79.
[31] Sun X, Zhang L, Tan H, Bao J, Strouthos C, Zhou X. Multi-scale agent-based brain cancer modeling and prediction of TKI treatment response: incorporating EGFR signaling pathway and angiogenesis. BMC Bioinform 2012;13:218.
[32] Pivonka P, Zimak J, Smith DW, Gardiner BS, Dunstan CR, Sims NA, et al. Model structure and control of bone remodeling: a theoretical study. Bone 2008;43:249–63.
[33] Lee JM, Gianchandani EP, Eddy JA, Papin JA. Dynamic analysis of integrated signaling, metabolic, and regulatory networks. PLoS Comput Biol 2008;4:e1000086.
[34] Komori T. Regulation of bone development and maintenance by Runx2. Front Biosci 2008;13:898.
[35] Isaksson H, van Donkelaar CC, Huiskes R, Ito K. A mechano-regulatory bone-healing model incorporating cell-phenotype specific activity. J Theor Biol 2008;252:230–46.
[36] Zhang Q, Chang Q, Cox RA, Gong X, Gould LJ. Hyperbaric oxygen attenuates apoptosis and decreases inflammation in an ischemic wound model. J Invest Dermatol 2008;128:2102–12.
[37] Ebbesen P, Eckardt K-U, Ciampor F, Pettersen EO. Linking measured inter-cellular oxygen concentration to human cell functions. Acta Oncol 2004;43:598–600.
[38] Wang Q, Wang J, Zhang X, Yu X, Wan C. Degradation kinetics of calcium polyphosphate bioceramic: an experimental and theoretical study. Mater Res 2009;12:495–501.
[39] Fernandez E, Gil F, Ginebra M, Driessens F, Planell J, Best S. Calcium phosphate bone cements for clinical applications. Part I: solution chemistry. J Mater Sci Mater Med 1999;10:169–76.
[40] Lu J, Descamps M, Dejou J, Koubi G, Hardouin P, Lemaitre J, et al. The biodegradation mechanism of calcium phosphate biomaterials in bone. J Biomed Mater Res 2002;63:408–12.
[41] Osher S, Fedkiw RP. Level set methods and dynamic implicit surfaces. 1st ed. New York: Springer Verlag; 2003119–24.
[42] Klipp E, Liebermeister W, Wierling C, Kowald A, Lehrach H. Systems biology: a textbook. Weinheim: Wiley-VCH; 200913–27.
[43] Morton KW, Mayers DF. Numerical solution of partial differential equations: an introduction. 2nd ed. New York: Cambridge Univ Pr; 200562–83.
[44] Artel A, Mehdizadeh H, Chiu YC, Brey EM, Cinar A. An agent-based model for the investigation of neovascularization within porous scaffolds. Tissue Eng Part A 2011;17:2133–41.
[45] Kang HS. Hierarchical design and simulation of tissue engineering scaffold mechanical, mass transport, and degradation properties. [PhD thesis]. Ann Arbor, MI: The University of Michigan. Online. 2012 Sep. Available from URL: http://141.213.232.243/handle/2027.42/78832; 2010.
[46] Davis H, Leach J. Designing bioactive delivery systems for tissue regeneration. Ann Biomed Eng 2011;39:1–13.
[47] Zandstra P, Petzer A, Eaves C, Piret J. Cellular determinants affecting the rate of cytokine depletion in cultures of human hematopoietic cells. Biotechnol Bioeng 1997;54:58–66.
[48] Lian JB, Stein GS. The developmental stages of osteoblast growth and differentiation exhibit selective responses of genes to growth factors (TGF beta 1) and hormones (vitamin D and glucocorticoids). J Oral Implantol 1993;19:95–105 [discussion 36–7].
[49] Lian JB, Stein GS. Development of the osteoblast phenotype: molecular mechanisms mediating osteoblast growth and differentiation. Iowa Orthop J 1995;15:118.
[50] Roy TD, Simon JL, Ricci JL, Rekow ED, Thompson VP, Parsons JR. Performance of degradable composite bone repair products made via three-dimensional fabrication techniques. J Biomed Mater Res A 2003;66:283–91.

[51] Story BJ, Wagner WR, Gaisser DM, Cook SD, Rust-Dawicki AM. In vivo performance of a modified CSTi dental implant coating. Int J Oral Maxillofac Implants 1998;13:749–57.

[52] Lewandrowski KU, Gresser JD, Bondre SP, Silva AE, Wise DL, Trantolo DJ. Developing porosity of poly (propylene glycol-co-fumaric acid) bone graft substitutes and the effect on osteointegration: a preliminary histology study in rats. J Biomater Sci Polym Ed 2000;11:879–89.

[53] Karageorgiou V, Kaplan D. Porosity of 3D biomaterial scaffolds and osteogenesis. Biomaterials 2005;26:5474–91.

[54] Kujala S, Ryhanen J, Danilov A, Tuukkanen J. Effect of porosity on the osteointegration and bone ingrowth of a weight-bearing nickel-titanium bone graft substitute. Biomaterials 2003;24:4691–7.

[55] Fisher JP, Vehof JWM, Dean D, van der Waerden JP, Holland TA, Mikos AG, et al. Soft and hard tissue response to photocrosslinked poly (propylene fumarate) scaffolds in a rabbit model. J Biomed Mater Res 2001;59:547–56.

[56] Leucht P, Kim J-B, Wazen R, Currey JA, Nanci A, Brunski JB, et al. Effect of mechanical stimuli on skeletal regeneration around implants. Bone 2007;40: 919–30.

[57] Patel ZS, Young S, Tabata Y, Jansen JA, Wong MEK, Mikos AG. Dual delivery of an angiogenic and an osteogenic growth factor for bone regeneration in a critical size defect model. Bone 2008;43:931–40.

[58] Shah NJ, Macdonald ML, Beben YM, Padera RF, Samuel RE, Hammond PT. Tunable dual growth factor delivery from polyelectrolyte multilayer films. Biomaterials 2011;32:6183–93.

[59] Young S, Patel ZS, Kretlow JD, Murphy MB, Mountziaris PM, Baggett LS, et al. Dose effect of dual delivery of vascular endothelial growth factor and bone morphogenetic protein-2 on bone regeneration in a rat critical-size defect model. Tissue Eng Part A 2009;15:2347–62.

[60] Kim S, Kang Y, Krueger CA, Sen M, Holcomb JB, Chen D, et al. Sequential delivery of BMP-2 and IGF-1 using a chitosan gel with gelatin microspheres enhances early osteoblastic differentiation. Acta Biomater 2012;8:1768–77.